J. E. Purkinje University in Ústí nad Labem

Faculty of Science

Department of Physics

Abstract of the Doctoral Thesis

ADVANCED MHD MODELLING OF PLASMA PROCESSES IN SOLAR PHYSICS

by

MGR. JAN SKÁLA

Ústí nad Labem, 2015

Univerzita J. E. Purkyně v Ústí nad Labem

Přírodovědecká fakulta

Katedra fyziky

Autoreferát disertační práce

POKROČILÉ MHD MODELOVÁNÍ PLASMOVÝCH PROCESŮ VE SLUNEČNÍ FYZICE

MGR. JAN SKÁLA

Ústí nad Labem, 2015

Disertační práce byla vypracovaná na základě vědeckých výsledků na katedře fyziky Přírodovědecké fakulty Univerzity J. E. Purkyně v Ústí nad Labem v letech 2008-2015 v rámci doktorského studia P1703 Počítačové metody ve vědě a technice.

Doktorand: Mgr. Jan Skála

Školitel: Mgr. Miroslav Bárta, Ph.D.
                    Astronomický ústav AV ČR
                    Fričova 298, 251 65 Ondřejov

Oponenti: doc. RNDr. Marian Karlický, DrSc.
                    Astronomický ústav AV ČR
                    Fričova 298, 251 65 Ondřejov

                    Dr. Bernd Inhester
                    Max Planck Institute for Solar System Research
                    Justus-von-Liebig-Weg 3, 370 77 Göttingen

Autoreferát byl odevzdán dne
Tento autoreferát je online dostupný na adrese:
http://sci.ujep.cz/doktorskestudium-info.html

Obhajoba se koná dne   v   hodin před komisí pro obhajoby disertačních prací v oboru P1703 Počítačové metody ve vědě a technice na Přírodovědecké fakultě Univerzity J. E. Purkyně v Ústí nad Labem, místnost   , České mládeže 8, 400 96 Ústí nad Labem.

S disertací je možno se seznámit na studijním oddělení Přírodovědecké fakulty Univerzity J. E. Purkyně v Ústí nad Labem.

Předseda OR: prof. RNDr. Rudolf Hrach, DrSc.
                    Katedra fyziky, PřF, UJEP
                    České mládeže 8, 400 96 Ústí nad Labem

Abstract

Although the finite element method (FEM) is well established tool of numerical modelling in the material research and in the engineering applications of the fluid dynamics, applications in the magneto-hydrodynamics (MHD) and, especially, in the astrophysical plasmas are recently only slowly developing. Nevertheless, contrary to commonly used finite difference methods, the FEM has many advantages – above all, more precise implementation of boundary conditions and unstructured mesh.

The main goal of this work is to implement parallel (MPI) MHD code based on the FEM and its application to the problem of the interaction of the scales in the magnetic field reconnection in a solar flare. The theoretically expected cascade in the turbulent reconnection will be studied using the developed code. The final result should be to understand energy transfer from global scale of eruption into the dissipative micro-scale and, conversely, relations between changes in the connectivity of dissipative-scale magnetic field and global change in the topology of magnetic field in an active region.

Abstrakt

Zatímco v materiálovém výzkumu a inženýrské hydrodynamice jsou metody konečných prvků (FEM) dobře etablovaným nástrojem numerického modelování, v magnetohydrodynamice (MHD) a především jejích astrofyzikálních aplikacích se začínají teprve zvolna rozvíjet. Přitom oproti užívaným metodám konečných diferencí mají mnoho předností – především přesnější implementaci hraničních podmínek a nestrukturovanou síť.

Cílem práce je vytvoření paralelního (MPI) MHD kódu založeného na metodě konečných prvků a jeho použití především na řešení problému interakce škál v procesu rekonexe magnetického pole ve sluneční erupci. S pomocí vytvořeného kódu bude studována teoreticky předpokládaná kaskáda v turbulentní rekonexi. Konečným výstupem by mělo být porozumění přenosu energie od globální škály erupce směrem k disipativní mikroškále a naopak souvislost změn konektivity magnetického pole na úrovni disipativní škály s globálními změnami magnetické topologie v aktivní oblasti.

Introduction

Dynamics of magnetized plasma at sufficiently large spatial and temporal scales can be adequately described by the set of magnetohydrodynamic (MHD) equations (Priest, 1984). In many problems we face the situation with high Lundquist (a.k.a. magnetic Reynolds) number

$$S \equiv Re_{\mathrm{M}} = L\mu_{\mathrm{o}}V_{\mathrm{A}}/\eta \ ,$$

where L is the characteristic size of the system, $V_{\mathrm{A}} = B/\sqrt{\rho}$ the typical Alfvén velocity (B and ρ being the magnetic field strength and plasma density, respectively) and η the electric resistivity. A direct consequence of the high Lundquist number is a large separation between the system size and the dissipation scale. The cascading fragmentation of the current layer in the magnetic reconnection in solar flares (Shibata and Tanuma, 2001; Bárta et al., 2011b,a) can serve as an example of such a multi-scale problem: The span between the eruption size ($\approx 10^5$ km) and the dissipation scale (1 m – 10 m) in the practically collision-less coronal plasmas easily extends seven orders of magnitude.

In general, there are two approaches how to handle such a broad range of scales. The first one uses a moderate numerical resolution and models the physics on the sub-grid (unresolved) scales using some plausible assumptions on the micro-scale statistical properties (correlations) of the quantities that define the system (e.g. flow or magnetic field). Among them, e.g., the large-eddy simulations (LES) (Mátais, 2001) or Reynolds-averaged numerical simulations (RANS) (Leschziner, 2001) belong to the well known methods used widely in engineering applications in the fluid dynamics.

The second approach is based on direct simulations that cover all the scales contained in the problem. Traditionally, the adaptive mesh refinement (AMR) technique is used with the finite-difference/finite volume methods in order to resolve high-gradient regions locally, keeping the total number of grid points required for simulation at a manageable level (see, e.g., Berger and Oliger, 1984; Fryxell et al., 2000; van der Holst and Keppens, 2007).

Nevertheless, also this approach has its limitations caused by introduction of artificial boundaries between fine and coarse meshes. This problem, however, can be cured by the methods based on un-

structured mesh, such as is used in FEM. With this in mind we have implemented a FEM-based solver for MHD equations and present it in the current paper. From various FEM formulations we have chosen the least-squares FEM (LSFEM) because it is robust, universal (it can solve all kinds of partial differential equations) and it is efficient – it always leads to the system of linearized equations with symmetric, positive definite matrix (Jiang, 1998). The LSFEM keeps many key properties of the Rayleigh-Ritz formulation even for systems of equations for which the equivalent optimization problem (in Rayleigh-Ritz sense) does not exist (Bochev and Gunzburger, 2009).

Despite of the FEM applications in the fluid dynamics made a substantial development in the past years, its usage for numerical solution of MHD equations is still rather rare. For example, the *NIMROD* (Sovinec et al., 2004) and *M3D* codes (Jardin and Breslau, 2005) – based on Galerkin formulation – belong to a few known implementations of FEM-based MHD solvers. Related work also has been done by Lukin (2008) who implemented the MHD (and two-fluid) equations within the more general code framework SEL (Glasser and Tang, 2004) based on the Galerkin formulation with high-order Jacobi polynomials as the basis functions.

Method

In general, LSFEM is formulated for the linear problem

$$\mathcal{A}\boldsymbol{u} = \boldsymbol{f} \qquad \text{in } \Omega$$

$$(1)$$

$$\mathcal{B}\boldsymbol{u} = \boldsymbol{g} \qquad \text{on } \Gamma = \partial\Omega$$

where $\mathcal{A}$ is the linear (differential) operator, $\mathcal{B}$ the boundary operator, Ω is the domain and Γ is the boundary of Ω, $\boldsymbol{f}$ is a source vector and $\boldsymbol{g}$ is a boundary condition.

In the least-square formulation of the FEM the problem described by Eqs. (1) is transformed to seek the minimum of the functional

$$\int_{\Omega_e} \mathcal{A}^T \Phi_i \mathcal{A} \Phi_j \mathrm{d}\Omega + h^{-1} \int_{\Gamma_e} \mathcal{B}^T \Phi_i \mathcal{B} \Phi_j \mathrm{d}\Gamma =$$

$$\int_{\Omega_e} \mathcal{A}^T \Phi_i \boldsymbol{f} \mathrm{d}\Omega + h^{-1} \int_{\Gamma_e} \mathcal{B}^T \Phi_i \boldsymbol{g} \mathrm{d}\Gamma, \quad (2)$$

where h^{-1} is appropriate mesh-dependent weighting factor (Bochev and Gunzburger, 2009), function $\boldsymbol{u} = \sum \Phi_j \boldsymbol{u}_j$ is approximated by a set of unknown parameters $\boldsymbol{u}_j$ and *basis* (trial) functions $\Phi_j(\boldsymbol{x})$ where $\boldsymbol{x}$ is an independent variable..

Generally, the operators from formal LSFEM problem (1) are in the nonlinear form. We need transform operators into the linear and time discretized form for computational purposes. The linearization of operator can be achieved straightforwardly by lagging the nonlinear term. This simple iteration method (also called successive substitution method) has slow convergence. To improve rate of convergence, we can apply the Newton-Raphson linearization method due to its quadratic convergence (see Dennis and Schmabel (1996)). The Newton-Raphson (N-R) method is a powerful and widely used technique for solving nonlinear equations numerically. Let consider a system of partial differential equations in the conservative form

$$\frac{\partial \boldsymbol{\Psi}}{\partial t} + \frac{\partial \boldsymbol{F}_i}{\partial x_i} = 0 , \qquad (3)$$

where $\boldsymbol{F}_i$ is a flux in the direction of coordinate x_i and $\boldsymbol{\Psi}$ is a state vector (note that the MHD equations can be re-written into this form

as well). Then the operator $\mathcal{A}$ from equation (2) for the conservative hyperbolic equation (3) reads

$$\mathcal{A} = 1 + \Theta \Delta t \left(\frac{\partial \boldsymbol{A}_i^k}{\partial x_i} + \boldsymbol{A}_i^k \frac{\partial}{\partial x_i} \right) \tag{4}$$

where parameter $\Theta \in \langle 0, 1 \rangle$ controls the implicitness of the scheme, $\boldsymbol{A}_i^k = \left. \frac{\partial \boldsymbol{F}_i}{\partial \boldsymbol{\Psi}} \right|_k$ is the Jacobian matrix, index k denotes N-R linearization iteration step, and corresponding right hand side (RHS) has the following form

$$\boldsymbol{f} = \overline{\boldsymbol{\Psi}}_1 - (1 - \Theta) \Delta t \left(\frac{\partial \overline{\boldsymbol{F}}_i}{\partial x_i} - \frac{\partial \boldsymbol{A}_i^k}{\partial x_i} \boldsymbol{\Psi}^k \right) , \tag{5}$$

where terms with over-line are from the old time step. The complete linearized operator and RHS for one fluid resistive MHD equitations are shown in expanded form in the Appendix of the thesis.

LSFEM implementation of MHD

At the first we divide the global domain into elements. We use triangle elements in whole domain. The method of mesh creation has been described by Chung (2002). The second step is mapping a shape functions on the created mesh – creating a function space.

Next part of initialization is initial condition. The state vector of each node has set values according to its global spatial coordinates.

When we have initial mesh and function space we can continue into the main loop of the code. The top loop is counting a time. It controls the time step size Δt and contains nested linearization loop, Gaussian integration, assembling sparse stiffness matrix and load vector, and solving a system of linear equations. The time step is set according to the Courant-Friedrichs-Lewy condition. The nested loop is over linearization. It finds solution of the sparse stiffness matrix and checks difference between a solution of the last linearization. If it is under the required accuracy $\frac{|\boldsymbol{u}^k - \boldsymbol{u}^{k+1}|}{|\boldsymbol{u}^{k+1}|} < \varepsilon$ the program continues to the next time step. The linearization loop usually finishes in 2-3 steps when the accuracy 10^{-8} is reached. The stiffness matrix assembling and solving is nested in the linearization loop. The stiffness matrix is assembled element by element. In the inner element loop we integrate terms in Eq. (2). The Gaussian quadrature (Chung, 2002) is used for

an integration where the transformation into natural triangle coordinatesis applied (Rathod et al., 2004). For faster evaluation of integrals we calculate and store operators applied on each interpolation (basis) function for given Gaussian point $\mathcal{A}\Phi_i$. We add the multiplied operators $\mathcal{A}^T\Phi_i \boldsymbol{W}\mathcal{A}\Phi_j$ into the stiffness matrix in positions according to the global node indexes and also we add multiplied operator with right hand side $\mathcal{A}^T\Phi_i \boldsymbol{W}\boldsymbol{f}$ into the load vector. The weighting diagonal matrix $\boldsymbol{W}$ sets the weights to the corresponding MHD equations and supplemental solenoidal condition $\nabla \cdot \boldsymbol{B} = 0$. After summming the sub-matrices and the sub-vectors for all Gaussian points we continue to the next element until the entire *stiffness matrix* and the *load vector* are assembled. The system of equations given by the stiffness matrix and the load vector is solved by the Jacobi preconditioned Conjugate Gradient Method (JCGM) (Press et al., 2007). The JCGM usually takes few tens of iteration to reach required precision (10^{-10}), where the speed of convergence (almost) do not depend on the size of the matrix. If the solenoidal condition is involved in the MHD equations (i.e. the corresponding weight from $\boldsymbol{W}$ is non-zero and we solve overdetermined system) then the condition number of stiffness matrix significantly increases (i.e. from $\sim 10^0$ to $\sim 10^4$) and the JCGM takes $10-50$ times more iterations. After obtaining solution from JCGM the program continues to the next linearization loop. The entire algorithm can be summarized as follows:

- time loop – adapt time step size according to CFL condition, check final desired time

    - linearization loop – if $\frac{|\boldsymbol{u}^k - \boldsymbol{u}^{k+1}|}{|\boldsymbol{u}^{k+1}|} < \varepsilon$ or maximum iteration count is reached continue to next time step

        - assembling stiffness matrix $\boldsymbol{K}$ element by element

            - integration by Gaussian quadrature

                1. compute the operator matrices for each basis function
                2. multiply the operator matrices then add the result into stiffness matrix
                3. multiply the operator matrix by the RHS then add result into the load vector

            - next Gaussian point
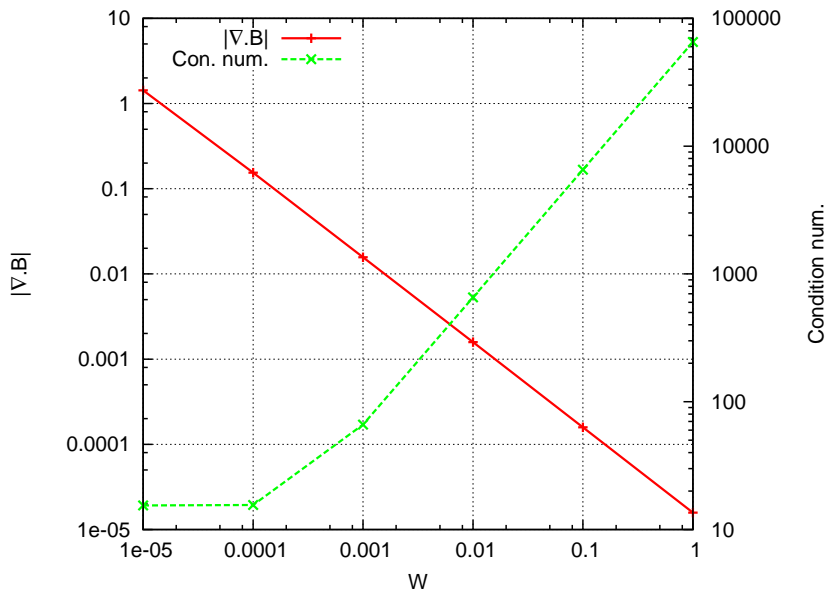   - next element

Figure 1 – The value of $\nabla \cdot \boldsymbol{B}$ and the condition number of stiffness matrix for various weights W for the solenoidal condition at the time $t = 0.1$. The simulation was performed using a homogeneous mesh consisting of $2 \times 128 \times 128$ triangle elements.

- – find new solution $\boldsymbol{u}^{k+1}$ of stiffness system by the JCGM
- – next linearization

- – next time step

Magnetic divergence suppression

Figure 1 shows dependency of divergence $\boldsymbol{B}$ and condition number of stiffness matrix on the weight of the solenoidal condition in the MHD equations. The graph shows an inverse relationship between weight and absolute value of divergence of magnetic field (integrated over whole domain). As we expect according to the minimization of residual error of the divergence $\boldsymbol{B}$ equation, the increasing weight reduces the magnetic charge in the domain. On the other hand, the raising weight significantly increases the condition number of the stiffness matrix and makes it difficult to solve.

The condition number is constant for the weight smaller than 10^{-4}. It is caused by a small contribution of divergence equation to the stiffness matrix. Unfortunately, the condition number steeply grows with the increasing weight, when the weight is greater than 10^{-4}. In these cases, the contribution to the operator matrix of $\nabla \cdot \boldsymbol{B}$ is significant

and it can even override other terms in the operator which leads to the increase of the condition number of the matrix.

Results

This section contains results obtained from the code both from the various testing/veryfication runs and the actual intended application to the problem of magnetic reconnection.

Ryu-Jones discontinuity test problem

Before application to the topical research problems the code has been tested on several benchmarks. As the first test we have run the standard Ryu-Jones ideal MHD 1D shock/discontinuity problem (Ryu and Jones, 1995). The initial state is given by prescriptions $(\rho, v_x, v_y, v_z, B_x, B_y, B_z, E) = (1, -1, 0, 0, 0, 1, 5, 1)$ in the left half, and $(\rho, v_x, v_y, v_z, B_x, B_y, B_z, E) = (1, 1, 0, 0, 0, 1, 5, 0)$ in the right half of the computational box, respectively. The domain $(-0.5, 0.5)$ was divided into 512 elements. We used the first order basis functions to approximate the FEM solution. The boundary conditions on both ends are of von Neumann type. Results at time $t = 0.1$ are shown in Fig. 2. They correspond and could be compared with Fig. 3b in Ryu and Jones (1995).
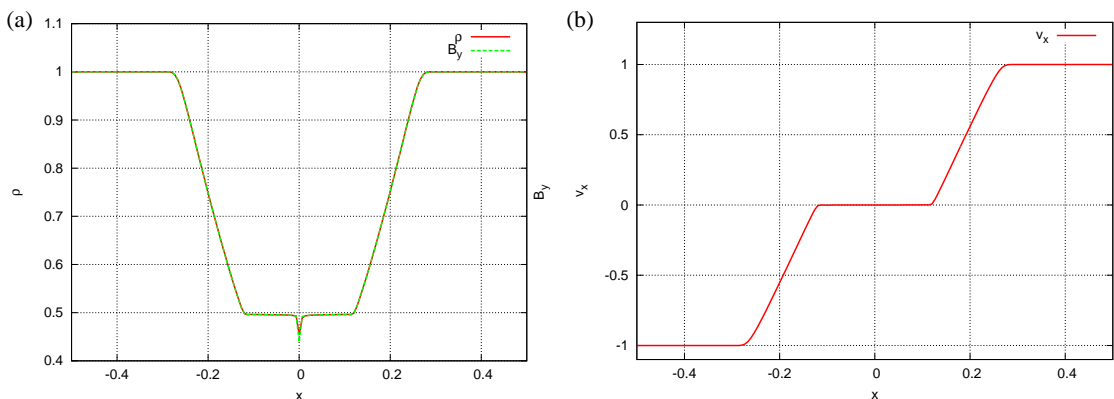

Figure 2 – The LSFEM solution of the MHD shock tube test (Ryu-Jones problem) at time $t = 0.1$ with the first-order basis functions. (a) density profile (red dashed line) and B_y profile along x-axis. (b) v_x profile along x-axis.

In order to study influence of basis-function order on the approximate solution we calculate the same test problem, now with the
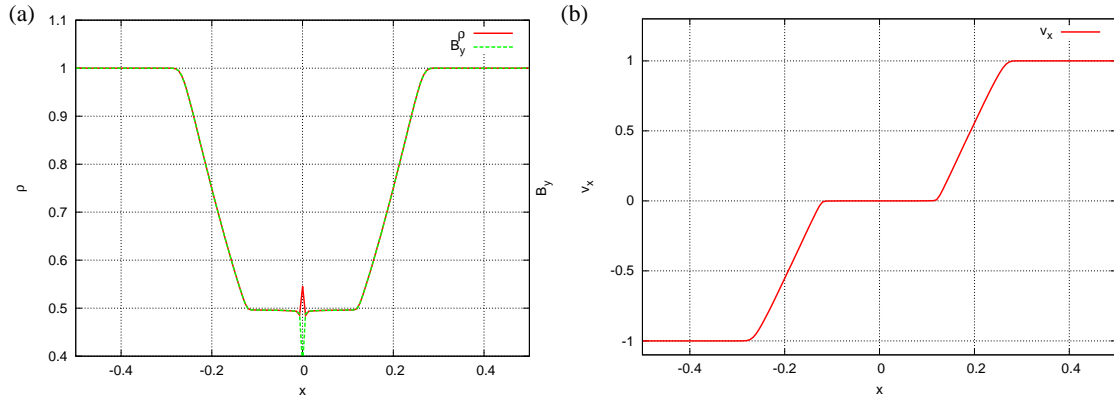
Figure 3 – The LSFEM solution of the MHD shock tube test (Ryu-Jones problem) at time $t = 0.1$ with the second-order basis functions. Displayed quantities are the same as in Fig. 2.

second-order Lagrange polynomials. All other parameters are the same as in the previous case displayed in Fig. 2. The results of second-order basis functions are shown in Fig. 3. Both simulations closely match to the expected profiles, only artificial peaks are developed in the middle of domain in density ρ and magnetic field B_y.

Orszag-Tang vortex test problem

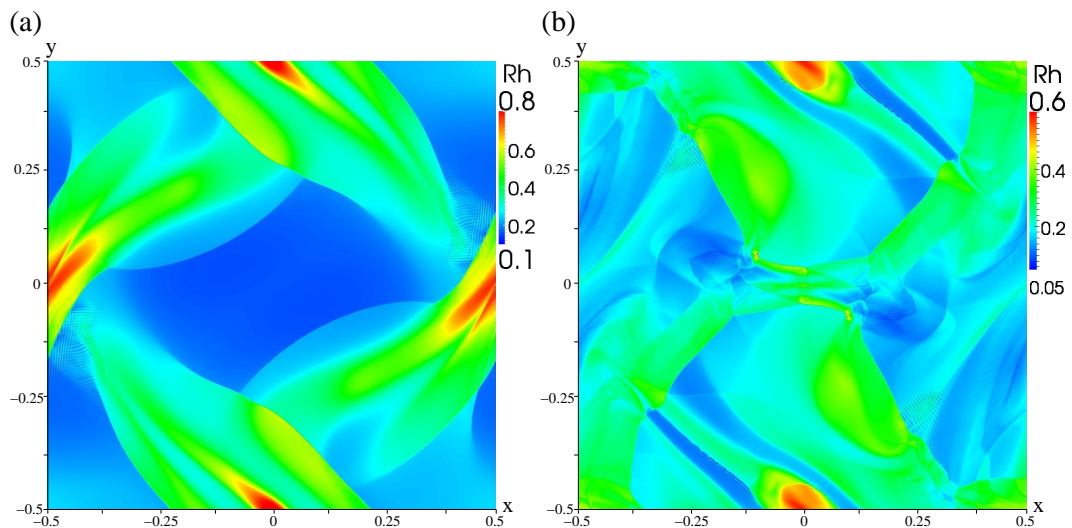As a next test, we performed the standard Orszag-Tang 2D ideal-MHD vortex problem (see Orszag and Tang, 1979).

Figure 4 – The Orzsag-Tang vortex. The color coded plasma density is displayed at time $t = 0.25$ (a) and $t = 0.50$ (b).
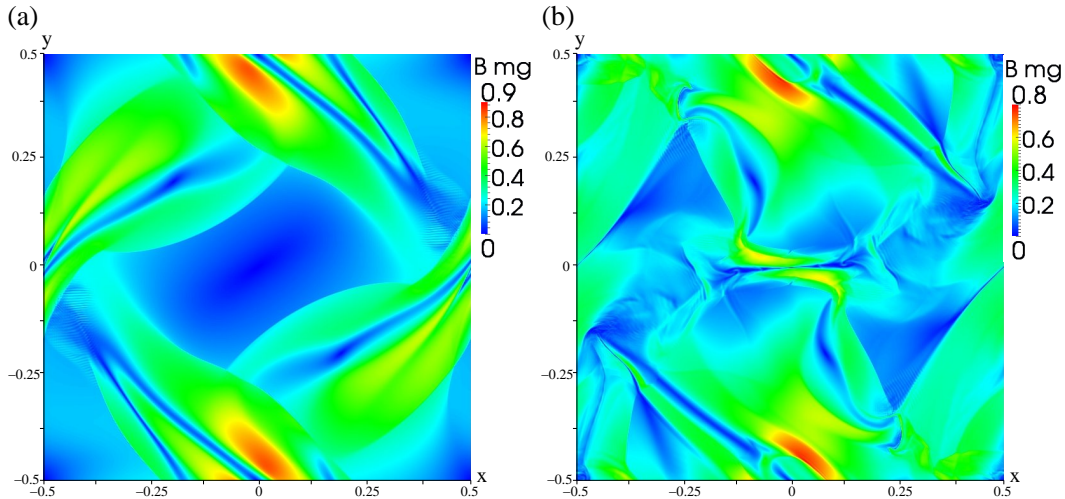
Figure 5 – The Orzsag-Tang vortex. The color coded magnitude of the magnetic field is displayed at times $t = 0.25$ (a) and $t = 0.50$ (b).

The computational domain 1.0×1.0 was discretized by $2 \times 640 \times 640$ triangular elements. We apply periodic boundary conditions at all boundaries. The first-order basis functions were used in this simulation. Results in Figs. 4 and 5 show the plasma density and the magnitude of the magnetic field, respectively, at times $t = 0.25$ (a), and $t = 0.50$ (b). The simulation reproduces classical Orszag-Tang structures only with small oscillations surrounding shock-fronts.

Resistive decay of a cylindric current

In order to assess the applicability of our code to the solutions of non-ideal (resistive) MHD problems and to estimate its numerical resistivity we performed a simulation of the resistive decay of a cylindrical current column in two spatial dimensions for which in certain limits analytical solutions exist (see Skála and Bárta, 2012).

Computational domain is divided into a homogeneous mesh of $2 \times 512 \times 512$ triangles in our numerical test. We use the first order basis functions to approximate the numerical solution. Free boundary conditions were applied on all boundaries. The results of this test are shown in Fig. 6. Fig. 6(a) shows time evolution of the current density profile along $y = 0$ for five subsequent time instants. Resistive decrease of j_z inside the column accompanied by formation of the induced surface current are well visible. Fig. 6(b) shows a comparison of numerical and
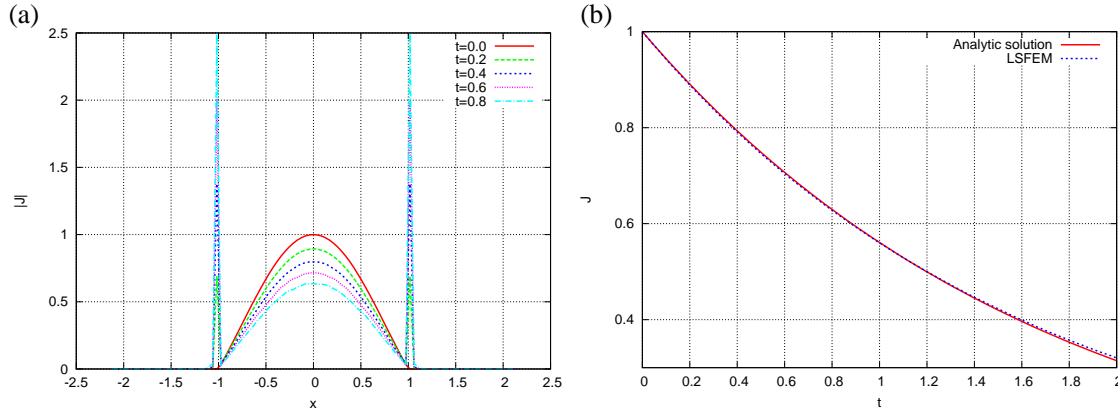
Figure 6 – A resistive decay of a cylindrical current density with time. (a) profiles of $j_z(x, 0, t)$ at five subsequent times. (b) The time profile of $j_z(0, 0, t)$ - comparison of numerical and analytical solutions.

analytical solutions for time evolution of the current density $j_z(x, y, t)$ at $x = 0, y = 0$. The plot reveals very good agreement between LSFEM and analytical solutions. Moreover, the induced current on the border of resistive disk does not spread further into the domain and stays only on the three boundary nodes between ideal and resistive plasma.

Magnetic field reconnection

Finally, after the benchmarking, we apply LSFEM implementation of the MHD solver for a numerical simulation of a real science case: The magnetic reconnection in a flare-like current sheet. The reference frame was chosen to have the y-axis in the vertical direction, the z-axis is in the invariant direction along the current density vector and the x-axis is perpendicular to the current sheet. The free von Neumann boundary conditions $\frac{\partial}{\partial \boldsymbol{n}} = 0$ are applied at the bottom, right and left sides except the normal component of magnetic field B_n. The component B_n is given by equation $\nabla \cdot \boldsymbol{B} = 0$. The mixed von Neumann and Dirichlet boundary conditions are applied on the bottom side. The Dirichlet boundary condition is applied to momentum density $\boldsymbol{\pi} = 0$ and tangential component of magnetic field $B_t = 0$ the other quantities are given by free von Neumann boundary conditions. The Dirichlet conditions ensures that the principal magnetic field component is vertical at the bottom boundary and the total flux passing through the boundary does not change, as enforce by the presence of

a dense solar photosphere (see Bárta et al. (2008)). The simulation box is set to $< -24, 24 > \times < -80, 80 >$. The domain is divided into homogeneous mesh with $2 \times 640 \times 2200 = 2.816 \cdot 10^6$ elements. The first order shape functions are mapped on the element. The plasma beta parameter used in simulations is $\beta = 0.15$ and the ratio of specific heats is $\gamma = 5/3$. The initial condition is set according to Harris-type current sheet (see Kliem et al. (2000))

The dynamical evolution of considered system is shown in figure 7. Evolution was triggered by small resistivity perturbation at middle of domain and then it causes a small burst of reconnection at the origin, which leads to acceleration of a plasma along the current sheet (y axis) by Lorentz force, see Fig. 7 - time $t = 10$. According to mass conservation the inflow is enforced into the region of initial perturbation. This convects a new magnetic flux toward the current sheet, which leads to increase of the current density again. Since the current sheet is stretched and compressed enough, the anomalous resistivity threshold v_{cr} is exceeded and the resistivity is switched on at the origin around time $t \sim 60$. This forms a secondary Petschek-like reconnection, which breaks and re-joints more magnetic field lines. A newly reconnected field lines are pulled by the Lorentz force and form the outflows of heated plasma, which reach the Alfvén velocity after $t \sim 80$. The current sheet is continuously stretched by fast outflows. The long and thin current sheet formed the Sweet-Parker reconnection configuration and the anomalous resistivity is triggered in several locations simultaneously. Later, a new X-points are formed – the so-called secondary tearing. Around time $t \sim 100$, the plasmoids are formed and plasmoids are directed to boundaries with the outflows. The plasmoids are further accelerated then the fast shocks are formed in front of magnetic islands around time $t = 160$.
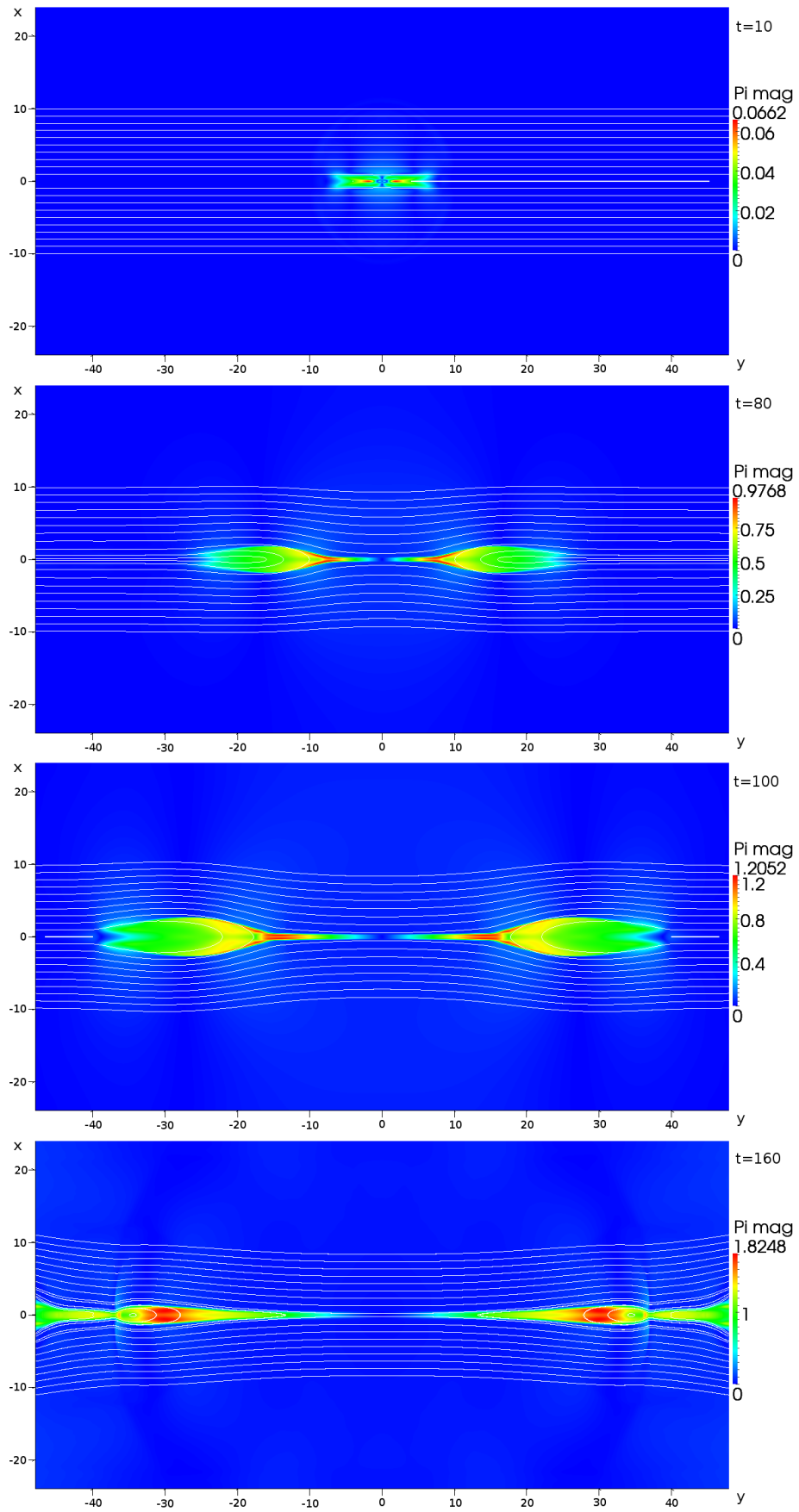
Figure 7 – The momentum density with the magnetic field lines at several times of evolution.

Conclusions

The FEM represents an alternative to FDM/FVM that are traditionally used for solution of MHD problems in astrophysics. Its attractivity implies from its unstructured mesh that allows for appropriate local refinement without formation of qualitative internal boundaries between the fine and coarse meshes.

We have developed the parallel MPI LSFEM implementation of a MHD solver with the adaptive mesh refinement.

We performed several standardized tests focused on an ideal and resistive MHD. The LSFEM MHD solver quite closely reproduces results published for the Ryu-Jones shock tube problem (Ryu and Jones, 1995). Small spurious oscillations appear around the points where the first derivative of an analytical solution does not exist. Choice of the higher-order basis functions makes the situation even slightly worse.

Similar feature can be seen in the results from the Orszag-Tang vortex test problem (Orszag and Tang, 1979). While the large-scale dynamics agree well with those obtained from the 'gauge' codes, small oscillations accompanying the shocks are visible again. These effects are caused by the least squares residual minimization in fixed norm, which cannot handle discontinuity and monotone solution on the same mesh (Bochev and Gunzburger, 2009).

Finally, we tested the properties of our implementation for solution of the resistive problems. In order to get a comparison with an analytical solution we have 'frozen' the plasma dynamics by setting high mass density and we concentrated on a purely diffusive problem. The results show a rather good agreement with the analytical solution. Namely, the induced surface current density is located only at three nodes and did not diffuse further with time. This is an important result for studies of the current-sheet filamentation in the flare reconnection.

The simulation of the Harris-like current sheet with the mesh refinement reproduces expected formation of the current sheet tearing with formation of plasmoids. Moreover this simulations reveals that there is no negative influence of the locally refined mesh on the numeric solution as partially reflected waves on the interface between coarse and finer mesh. As the numeric tests show, LSFEM has very small numeric diffusivity which leads to the bursty magnetic field re-

connection. The anomalous resistivity is localized to the very small region (corresponding to the concentrated current density according to the used resistivity model) which leads to the fast Petschek-like reconnection. The acceleration of the outflow and reconnected field lines by Lorenz force is not disturbed by numeric viscosity and the stretching of the current sheet is very fast. The long and stretched current sheet is prone to secondary tearing and then plasmoid formation.

The tests show basic applicability of our LSFEM implementation of the MHD solver for a solution of selected problems. At the same moment they reveal the necessity to involve both the adaptive spatial refinement and adaptive change of the order of basis functions over selected elements (h-p refinement). These features will be implemented into our code in a near future.

Shrnutí

FEM reprezentuje alternativu k FDM/FVM, které jsou tradičně používány na řešení MHD problémů v astrofyzice. Atraktivita metody vyplývá z její nestrukturované sítě, která umožňuje lokální zjemnění bez kvalitativního přechodu na vnitřní hranici mezi jemnou a hrubou sítí.

Vytvořili jsme MPI paralelní kód řešící MHD rovnice založený na LSFEM s adaptivním zjemňováním sítě.

Kód jsme testovali na několika standardních úlohách zaměřených na ideální i rezistivní MHD. LSFEM kód věrně zreprodukoval výsledky publikované Ryu and Jones (1995). Malé numerické oscilace se zformovaly v bodě, kde neexistuje konečná derivace. Použití bázových funkcí vyšších řádů nepatrně zvýšilo amplitudu oscilace.

Podobnou vlastnost můžeme pozorovat i ve výsledcích z testu 'Orszag-Tang vortex problem' (Orszag and Tang, 1979). Velkoškálová dynamika koreluje s výsledky obdrženými 'kalibračními' kódy, ale v blízkosti šokových vln můžeme pozorovat malé oscilace. Tyto efekty jsou způsobeny minimalizací rezidua metodou nejmenších čtverců, u které se stejnou normou nelze nalézt skokové a monotónní řešení na stejné síti.

Vlastnosti naší implementace metody byly testovány i na rezistivním problému. Abychom mohli porovnat numerické řešení s analytickým, tak jsme potlačili dynamiku plasmatu nastavením vysoké hustoty hmotnosti a tím jsme zredukovali MHD na čistě difuzní problém. Porovnání výsledků ukazuje shodu s analytickým řešením. Indukovaný plošný proud je popsán třemi uzly a v průběhu simulace nedifunduje. Toto je důležitý výsledek pro studium filamentace proudové vrstvy v rekonexi eruptivní oblasti.

Simulace Harrisovy proudové vrstvy se zjemněnou sítí zreprodukovala očekávaný rozpad proudové vrstvy a formování plazmoidů (magnetických ostrovů). Navíc tato simulace odhalila, že zjemněná síť nemá negativní vliv (například částečný odraz vln na rozhraní mezi jemnou a hrubou sítí) na numerické řešení. Numerický test ukázal, že LSFEM má velmi malou numerickou rezistivitu, což vede k impulsivní magnetické rekonexi. Anomální rezistivita je aplikována jen ve velmi malých oblastech (dle koncentrace hustoty elektrického proudu použitém v modelu anomální rezistivity), což vede k rychlé rekonexi podle Pet-

schekova modelu rekonexe. Akcelerace výtoků plazmatu a přepojených magnetických siločár není zpomalována numerickou viskozitou, a to způsobuje velmi rychlé natahování a stlačování proudové vrstvy. Dlouhá a stlačená proudová vrstva je náchylná na další rozpad proudové vrstvy a následnou tvorbu plazmoidů.

Testy ukázaly základní použitelnost LSFEM implementace MHD na řešení vybraných problémů. Zároveň odhalily nutnost zahrnutí prostorového zjemňování sítě a adaptivní změnu řádu bázových funkcí na vybraných elementech (h-p zjemňování sítě). Tyto vlastnosti budou implementovány do našeho kódu v blízké budoucnosti.

Reference

Bárta, M., Büchner, J., Karlický, M., Kotrč, P., Mar. 2011a. Spontaneous Current-layer Fragmentation and Cascading Reconnection in Solar Flares. II. Relation to Observations. ApJ730, 47.

Bárta, M., Büchner, J., Karlický, M., Skála, J., Aug. 2011b. Spontaneous Current-layer Fragmentation and Cascading Reconnection in Solar Flares. I. Model and Analysis. ApJ737, 24.

Bárta, M., Karlický, M., Žemlička, R., Dec. 2008. Plasmoid Dynamics in Flare Reconnection and the Frequency Drift of the Drifting Pulsating Structure. Sol. Phys.253, 173–189.

Berger, M. J., Oliger, J., Mar. 1984. Adaptive Mesh Refinement for Hyperbolic Partial Differential Equations. Journal of Computational Physics 53, 484–512.

Bochev, P. P., Gunzburger, M. D., 2009. Least-Squares Finite Element Methods. Springer Science+Business Media, LLC, 233 Spring Street, New York, NY 10013, USA.

Chung, T. J., Mar. 2002. "Computational Fluid Dynamics". Cambridge University Press.

Dennis, J. E. J., Schmabel, R. B., 1996. Numerical Methods for Unconstrained Optimization and Nonlinear Equations. Soc for Industrial & Applied Math.

Fryxell, B., Olson, K., Ricker, P., Timmes, F. X., Zingale, M., Lamb, D. Q., MacNeice, P., Rosner, R., Truran, J. W., Tufo, H., Nov. 2000. FLASH: An Adaptive Mesh Hydrodynamics Code for Modeling Astrophysical Thermonuclear Flashes. ApJS131, 273–334.

Glasser, A. H., Tang, X. Z., Dec. 2004. The SEL macroscopic modeling code. Computer Physics Communications 164, 237–243.

Jardin, S. C., Breslau, J. A., May 2005. Implicit solution of the four-field extended-magnetohydrodynamic equations using high-order high-continuity finite elements. Physics of Plasmas 12 (5), 056101.

Jiang, B., 1998. The Least-Squares Finite Element Method. Springer-Verlag Berlin Heidelberg, Springer-Verlag Berlin Heidelberg, Germany.

Kliem, B., Karlický, M., Benz, A. O., Aug. 2000. Solar flare radio pulsations as a signature of dynamic magnetic reconnection. A&A360, 715–728.

Leschziner, M. A., 2001. Course 4: Statistical Turbulence Modelling for the Computation of Physically Complex Flows. In: Lesieur, M., Yaglom, A., David, F. (Eds.), New Trends in Turbulence. p. 187.

Lukin, V. S., Jan. 2008. Computational study of the internal kink mode evolution and associated magnetic reconnection phenomena. Ph.D. thesis, Princeton University, Princeton, New Jersey 08544 USA.

Mátais, O., 2001. Course 3: Large-Eddy Simulations of Turbulence. In: Lesieur, M., Yaglom, A., David, F. (Eds.), New Trends in Turbulence. pp. 113–186.

Orszag, S., Tang, C., 1979. Small-scale structure of two-dimensional magnetohydrodynamic turbulence. J. Fluid Mech. 90, 129.

Press, W. H., Teukolsky, S. A., Vetterling, W. T., Flannery, B. P., 2007. Numerical Recipes. Cambridge University Press, The Edinburgh Building, Cambridge CB2 8RU, UK.

Priest, E. R., 1984. Solar magneto-hydrodynamics. Geophysics and Astrophysics Monographs, Dordrecht: Reidel, 1984.

Rathod, H. T., Nagaraja, K. V., Ramesh, N. L., 2004. Gauss Legendre quadrature over a triangle. J Indian Inst Sci 84, 183–188.

Ryu, D., Jones, T. W., Mar. 1995. Numerical magetohydrodynamics in astrophysics: Algorithm and tests for one-dimensional flow. ApJ442, 228–258.

Shibata, K., Tanuma, S., Jun. 2001. Plasmoid-induced-reconnection and fractal reconnection. Earth, Planets, and Space 53, 473–482.

Skála, J., Bárta, 2012. LSFEM Implementation of MHD Numerical Solver. Applied Mathematics 3 (11), 1842–1850.

Sovinec, C. R., Glasser, A. H., Gianakon, T. A., Barnes, D. C., Nebel, R. A., Kruger, S. E., Schnack, D. D., Plimpton, S. J., Tarditi, A., Chu, M. S., Mar. 2004. Nonlinear magnetohydrodynamics simulation using high-order finite elements. Journal of Computational Physics 195, 355–386.

van der Holst, B., Keppens, R., Sep. 2007. Hybrid block-AMR in cartesian and curvilinear coordinates: MHD applications. Journal of Computational Physics 226, 925–946.

Publications in impacted journals

Bárta, M., Büchner, J., Karlický, M., Skála, J., Aug. 2011. Spontaneous Current-layer Fragmentation and Cascading Reconnection in Solar Flares. I. Model and Analysis. ApJ737, 24.

Skála, J., Baruffa, F., Büchner, J., Rampp, M., Aug. 2015. The 3D MHD code GOEMHD3 for astrophysical plasmas with large Reynolds numbers. Code description, verification, and computational performance. A&A580, A48.

Other publications

Skála, J., Bárta, 2012. LSFEM Implementation of MHD Numerical Solver. Applied Mathematics 3 (11), 1842–1850.

Skála, J., Bárta, M., Varady, M., 02/02/2009 – 06/02/2009. Modelování rekonexe magnetických polí ve sluneční koróně metodou konečných prvků. In: Seminář numerické analýzy a zimní škola SNA'09 - Modelování a simulace náročných technických problémů. Ústav geoniky AV ČR Ostrava, iSBN 978-80-86407-60-9.

Skála, J., Bárta, M., Varady, M., 2011. MHD modelling of multi-scale magnetic reconnection using the Finite Element Method. Central European Astrophysical Bulletin 35, 195–204.

Skála, J., Bárta, M., Varady, M., 31/05/2010 – 04/06/2010. Modelování rekonexe magnetického pole pomocí metody konečných prvků.

In: Sborník příspěvků z 20. Celoštátného slnečného seminára. Papradno, SR, p. 84 – 89, iSBN: 978-80-85221-68-8.